# Behavior of X60 Line Pipe Subjected to Axial and Lateral Deformations

**Navid Nazemi**

**Sreekanta Das**[1]
Associate Professor
e-mail: sdas@uwindsor.ca

Department of Civil and Environmental Engineering,
University of Windsor,
Windsor, ON, N9B 3P4, Canada

*Buried pipelines may be subjected to various complicated combinations of forces and deformations. This may result in localized curvature, strains, and associated deformations in the pipe wall. As a result, wrinkle may form. The wrinkled pipeline may then develop a rupture in the pipe wall and lose its structural integrity if it is subjected to further sustained loads or deformations. Recently, laboratory tests on NPS6 steel pipes were undertaken at the University of Windsor to study the wrinkling and post-wrinkling behaviors of this NPS6 pipe when subjected to lateral load in addition to internal pressure and axial load. Four full-scale laboratory tests were conducted, and it was found that the application of lateral load on wrinkled pipe produces a wrinkle shape similar to that occurred in a field NPS10 line pipe. Complex test setup was designed and built for successful loading and completion of these tests. This paper makes a detailed discussion on the test setup, test method, loading and boundary conditions, instruments used, and test results obtained from this study.* [DOI: 10.1115/1.4001426]

*Keywords: line pipe, axial load, lateral load, internal pressure, wrinkle, rupture*

## 1 Introduction

The energy related industries in North America use steel pipelines as the primary mode for transporting natural gas, crude oil, and various petroleum products. In Canada alone, about 700,000 kM of energy pipelines are in operation. Many additional pipelines projects especially in West Canada and Alaska of various scales such as the Mackenzie Gas Project and Alaska Highway Pipeline are underway. The Alaska Highway Pipeline Project, which will run between Prudhoe Bay in Alaska to various parts of USA through Yukon, British Columbia, and Alberta, will alone cost about U.S. $20 billion [1]. The majority of these pipelines run below ground and in the arctic and subarctic regions.

Field observations of these buried pipelines indicate that it is not uncommon for geotechnical movements to impose large displacements on buried pipelines, resulting in large localized deformations, strain, and curvature in the pipe wall. Such displacements may be associated with river crossings, unstable slopes, or regions of discontinuous permafrost. Often the deformation of the pipe wall results in local buckling (called "wrinkling") and, in its post-buckling (post-wrinkling) range of response, wrinkle develops rapidly to a significant magnitude. This can occur under the loading conditions that may be idealized as combinations of variable internal pressure, compressive axial load, lateral load, and moment.

Several studies [2–9] were completed to understand how wrinkle in the field line pipe initiates and grows under monotonically increasing axisymmetric axial deformation and under monotonically increasing bending deformation with and without internal pressure. Typically, for this type of loading, the specimen will begin to buckle locally when the longitudinal stress reaches a magnitude in the vicinity of the yield stress [10]. The buckle then amplifies in an elastic-plastic manner and develops into a wrinkle of large amplitude as the specimen shortens and the load falls off. That is, the specimen "softens." The study by Das et al. [5] shows that a X52 grade wrinkled pipe subjected to monotonically increasing axisymmetric axial deformation and internal pressure may not rupture, and multiple wrinkles can form that look like an "accordion" shape (Fig. 1). Other studies by Das et al. [11,12] show that the wrinkled pipe may lose its structural integrity because of rupture formation in the wrinkle region, if it is subjected to elastic-plastic strain reversals due to axial and bending cyclic deformations that develop due to temperature variations, pressure fluctuations, and freeze-thaw cycles of the ground (Fig. 2).

The objective for the current study is to investigate the wrinkling behavior and failure mode in the wrinkle under combined lateral and axial loadings. The motivation of this study was due to the diagnosis and exposure of a wrinkle shape that looks like a cowboy hat, and the rupture that occurred in the wrinkle location of a field X60 grade NPS10 (line pipe with nominal diameter of 10 in. or 254 mm) energy pipeline with a wall thickness of 7.9 mm, as shown in Fig. 3. This field specimen was obtained from a segment on of the pipeline on an unstable slope. The operating pressure in that segment of the line pipe ranges from $0.3p_y$ to $0.35p_y$. The physical inspection of the NPS10 field line pipe showed physical marks of soil thrust and rubbing in the portion of the pipe just above the wrinkle, and therefore, it was felt that the pipe wall in that region was subjected to a lateral load (load not aligned to the longitudinal axis of the pipeline). However, the real load combination was not known. Das et al. [13] conducted one laboratory test on a X52 grade pipe to understand the possible load combination that may have caused the rupture in the field NPS10 line pipe. The test load and specimen end conditions could not be controlled systematically in that test though the final deformed shape showed some similarities with the field NPS10 pipeline. Thus, a detailed and carefully designed experimental research program was undertaken at the University of Windsor for better understanding of the load and boundary conditions that possibly produced a wrinkle and the rupture in the wrinkle region that look similar to the field NPS10 line pipe. Four full-scale laboratory tests on NPS6 (pipe with a nominal diameter of 6 in. or 152 mm) X60 grade pipe [14] specimens were successfully completed, and the results are discussed in this paper.

[1]Corresponding author.

Contributed by the Pressure Vessel and Piping Division of ASME for publication in the JOURNAL OF PRESSURE VESSEL TECHNOLOGY. Manuscript received November 28, 2008; final manuscript received March 8, 2010; published online April 28, 2010. Assoc. Editor: Shawn Kenny.

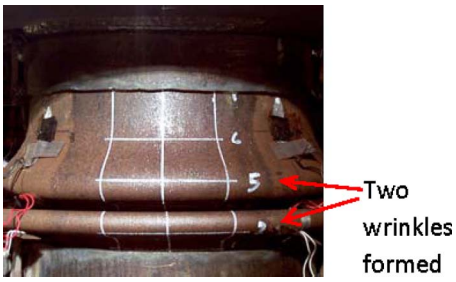


**Fig. 1 Accordion type failure under monotonic axial loading [5]**

## 2 Test Specimen and Test Setup

The test matrix used in this study is shown in Table 1. A total of four full-scale test specimens were made from 152 mm (6 in.) nominal diameter pipe made of API X60 grade steel. The actual yield strength ($\sigma_y$) for this pipe material at 0.5% strain was obtained from a coupon test and the value is 422 MPa (61.2 ksi). The modulus of elasticity of pipe steel ($E$) was 201 GPa. The outside diameter of the pipe was 168 mm with the diameter-to-thickness ratio ($D/t$) of 23 for this pipe. All test specimens were 800 mm long and had no girth weld (plain pipe). The ends of each pipe specimens were welded to 50 mm thick steel plates to contain the water and water pressure. The welding was done by a certified welder to ensure that no leaks occur in the welded locations during the load and pressure tests. The schematic of the test setup is shown in Fig. 4, and the picture of the actual test setup is shown in Fig. 5.

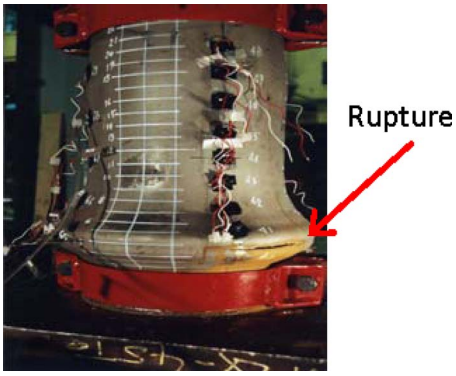


**Fig. 2 Rupture in the wrinkle due to cyclic axial deformation [11]**

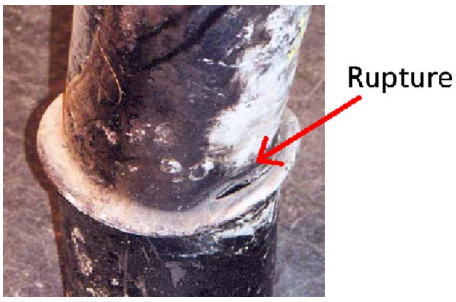


**Fig. 3 Shape of the wrinkle in the field NPS10 line pipe**

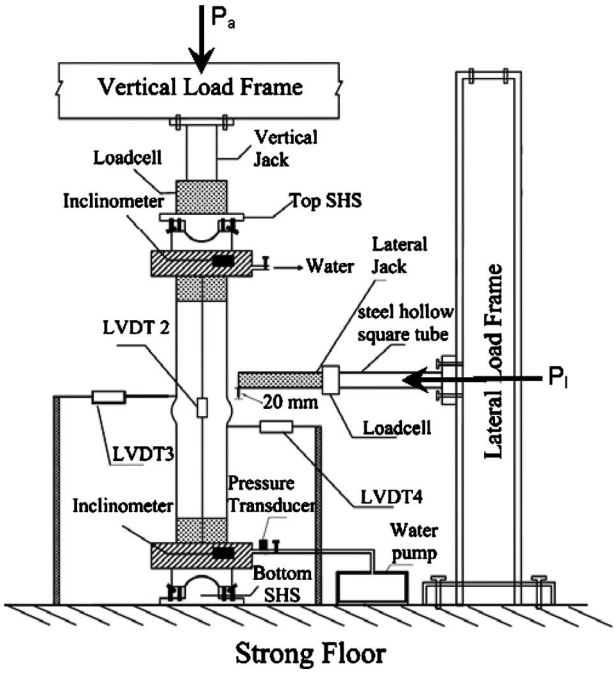


**Fig. 4 Schematic of the test setup**

The test setup was complex and required careful design and fabrication since the end conditions of the specimens were required to be changed between the pin and clamp when the specimen was under large loads. Special and complicated end conditions, which will be called as "swivel head support (SHS)," was designed, manufactured, and used to simulate both the pin and clamp end conditions, and to control the end rotations in the desired manner. The SHS has a male-female cup and cone type steel assembly with specially designed screws in between the two parts, as shown in Fig. 6. Each SHS is able to rotate up to 20 deg, and rotation can be frozen to any desired value by locking the rotating heads of special screws even when the pipe specimen is fully loaded and under internal pressure. One SHS at each end of the pipe specimen was mounted, as shown in Figs. 4 and 5.

Two loading jacks and load cells were used for application of the axial and lateral loads and deformations. The internal pressure was applied using an air-driven water pump. Two collars, each was 50 mm long and made of the same pipe material, were

**Table 1 Test matrix**

| | Main load test | | Pressure test | |
|---|---|---|---|---|
| Specimen | Normal pressure (Step 1-Step 2-Step 3) | End conditions | Maximum pressure (MPa) | End conditions |
| 1 | $0.3p_y-0.3p_y-0.3p_y$ | Fixed-pin-semipin | $5.1(0.14p_y)$ | Free at the top |
| 2 | $0.3p_y-0.3p_y-0.0p_y$ | Fixed-pin-fixed | $5.1(0.14p_y)$ | Free at the top |
| 3 | $0.15p_y-0.15p_y-0.15p_y$ | Fixed-pin-fixed | $6.1(0.17p_y)$ | Free at the top |
| 4 | $0.15p_y-0.15p_y-0.0$ | Fixed-pin-fixed | $5.9(0.16p_y)$ | Free at the top |

Note: End conditions at both ends during the main load test were same. The specimen was resting on floor during the pressure test.

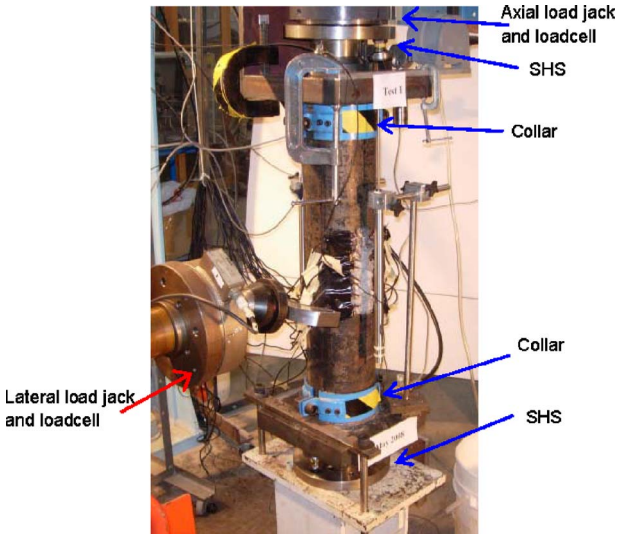


**Fig. 5 Picture of the test setup**

mounted at the ends of the pipe specimen to prevent any local buckling and/or rupture near the intersection of pipe and steel end plates.

## 3 Instrumentation

The load, deformation, internal pressure, and local strain data were acquired through an automatic data acquisition system and using appropriate instruments.

**3.1 Pressure.** An air-driven water pump of 31 MPa (4500 psi) capacity was used to apply the required internal pressure ($p_i$). The pressure was controlled and recorded through a pressure transducer, which was installed on the water supply line in between the pump and the bottom end plate (Fig. 4).

**3.2 Axial and Lateral Loads.** A 3000 kN capacity universal (compression-tension) hydraulic loading jack with a 3000 kN capacity universal load cell was used to apply, control, and acquire the axial load ($P_a$) data. Another universal hydraulic loading jack and load cell of 800 kN were used to apply, control, and acquire the lateral load ($P_l$) (Fig. 4).

**3.3 Rotations.** An inclinometer is an instrument for measuring the angles of slope or inclination of an object with respect to the gravity. Two inclinometers were mounted and used to control and acquire the rotation history at the top and bottom ends of the pipe specimen. The inclinometers were mounted on the end capping steel plates, which were welded to the pipe specimen (Fig. 4). The inclinometers were used to measure the angle of rotation in the direction of application of the lateral load. Two manual digital rotation meters were also mounted to record the end rotations of the specimen in the perpendicular direction.

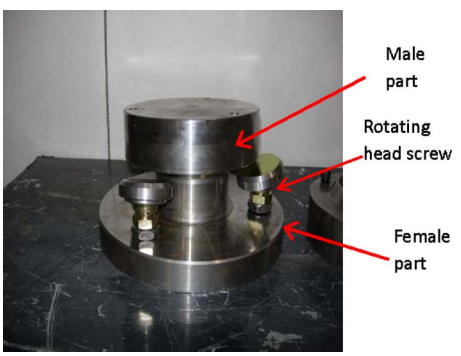


**Fig. 6 Swivel head support assembly**

**3.4 Displacements.** The linear variable differential transformer (LVDT) was used for measuring displacement. Four LVDTs with a maximum travel of 150 mm were mounted and used to control and acquire the deformation data. Two of these LVDTs (second LVDT or LVDT 2 is shown in Fig. 4) were used to control and acquire the vertical displacement of the specimen. Two other LVDTs (shown as LVDT 3 and LVDT 4) were mounted and used to acquire the lateral displacements: one was mounted on the face, where the lateral load was applied, and the other one was mounted on the opposite face of the pipe specimen.

**3.5 Strains.** Electrical resistance strain gauges (which will be called as "strain gauge" in the subsequent discussions) of 5 mm gauge length and 120 ohm resistance were installed on each pipe specimen for acquiring local strain data in and around the wrinkle. Since the exact location of the wrinkle is not quite predictable, a large number of strain gauges was used for each specimen. The total length of the strain gauge was 9 mm and actual gauge length was only 5 mm, and therefore, the strain gauges were installed in two vertical lines at 20 mm apart in a staggered manner to make best effort to capture the strain history at every critical point in the wrinkle region.

## 4 Test Procedure

A complex load-deformation history was applied. Two loads and/or deformations and internal pressure were required to be controlled simultaneously, and the boundary condition was required to be changed as well. Each test comprised of two major steps: (i) main load test when the specimen was loaded with the desired internal pressure, axial load, and lateral load, and (ii) pressure test when the specimen was subjected to an increasing internal pressure only without any axial and/or lateral loads. The objective of the main load step was to simulate the load and displacement conditions that the field NPS10 line pipe might have experienced either during its operation or during its shutdown period. The pressure test was then undertaken after unloading the axial and lateral loads, and internal pressure to simulate what might have happened soon after the field line pipe was being brought back to normal operation after its regular shutdown.

The main load test consisted of three load steps: (a) load step 1: axisymmetric axial deformation of about 40 mm, (b) load step 2: lateral load of 30–100 kN until a total end rotation was in the range of 5–6 deg, and (c) load step 3: further axial deformation of about 40 mm. Finite element analyses were undertaken to decide theses displacements and rotations before the test setup was built and tests were undertaken. Load-deformation behavior for specimens 4 and 2 are shown in Figs. 7 and 8, respectively. Internal pressures of 5.5 MPa (800 psi), which is equivalent to $0.15p_y$, and 11.0 MPa (1600 psi), which is equivalent to $0.30p_y$, were applied to these specimens, respectively before applying any other loads and specific end conditions. In load step 1, shown as "step 1" in these figures, an axisymmetric axial load ($P_a$) and deformation was applied using the vertical load jack (see Figure 4) until a total deformation of about 40 mm was achieved. It was found that a bulge type wrinkle of good size formed due to the application of this deformation, as shown in Fig. 9($a$) for specimen 4. During this loading stage, the two ends of the pipe specimen were kept clamped by tightening the screws of SHSs, and the internal pressure was kept unchanged.

In the next load step (load step 2) and shown as "step 2" in Figs. 7 and 8, the screws of the SHSs were loosened to simulate the pin end conditions at both ends so that the pipe specimen was able to rotate. The wrinkled section of a field line pipe can experience similar rotation if a mild reverse curvature forms on either side (upstream and downstream sides) of the wrinkle. The internal pressure was kept unchanged. Then, the lateral load jack was

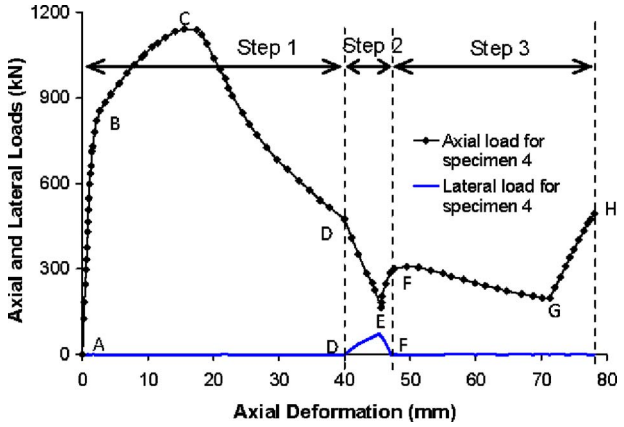


Fig. 7 Load-deformation behavior of specimen 4

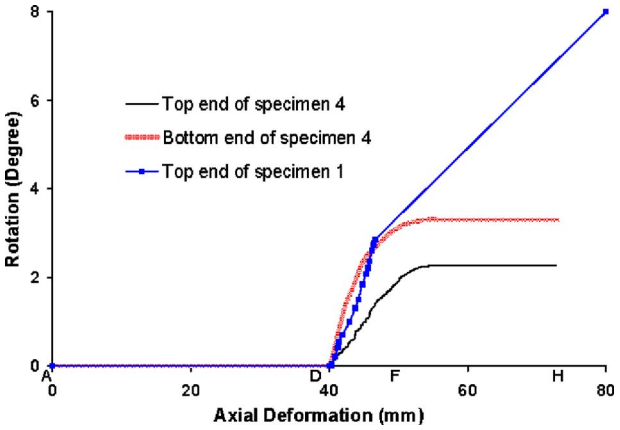


Fig. 10 Axial deformation-end rotations of specimens 1 and 4

mounted 20 mm above the top foot of the wrinkle (Fig. 4), and the lateral load was applied to a value of 30–100 kN until a total end rotation of about 5–6 deg was achieved. As a result, the pipe specimen developed a slight bent configuration, as shown in Fig. 9(*b*) for specimen 4.

In the last load step or load step 3, the end conditions were changed from pined-pined to clamped-clamped as they were in load step 1 to prevent any further rotation to occur at the ends of the pipe specimen. However, for specimen 1, being the first test using the specially designed SHSs, the end rotations could not be fully controlled in load step 3 because of the slacks in the rotating head screws used in between the male and female parts. As a result, the rotations continued to increase, and at the end of load step 3, the total rotation for this specimen became 19 deg, which was much higher than desired rotation of 5–6 deg. Therefore, the SHSs were modified by adding three more screws without rotating heads, and as a result, the rotations of the remaining three specimens could be controlled appropriately.

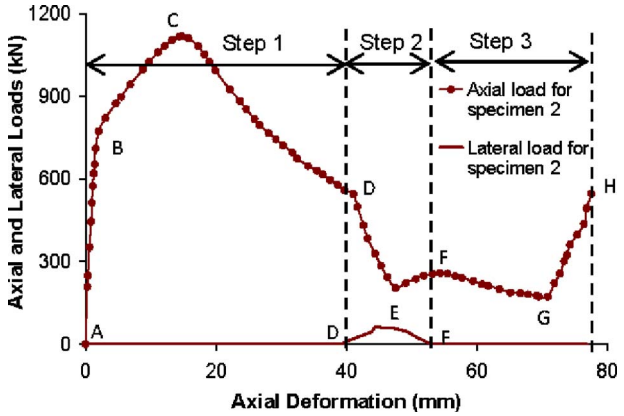


Fig. 8 Load-deformation behavior of specimen 2

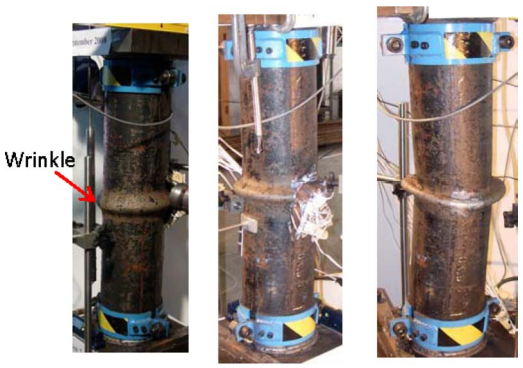


Fig. 9 Deformed shape of specimen 4 at the end of various load steps

Figure 10 shows the axial deformation-end rotations for specimens 1 and 4. Two inclinometers, one on the top end plate and the other one on the bottom end plate, were mounted for measuring the rotations at both ends of all specimens. However, for specimen 1, the bottom inclinometer did not function properly and could not be diagnosed during the test. As a result, no rotation data are available for the bottom end of specimen 1. However, after end of load step 3, the final rotation at the bottom end for specimen 1 was measured using a manual digital rotation meter, and it was 11 deg. The inclinometers for specimen 1 were removed after end of load step 2 (application of lateral load) because of the fear that the inclinometers may get damaged with further load application to the specimen. However, for other specimens, both inclinometers were left on the specimen until the end of load step 3.

The internal pressure was either reduced to zero or kept unchanged during load step 3, as shown in Table 1. For specimens 2 and 4, the internal pressure was reduced to zero, and the internal pressure for other two specimens (specimens 1 and 3) were not changed during this load step. The objective of changing pressure for specimens 2 and 4 in load step 3 was to simulate the shutdown condition of the field pipeline and to study the effect of absence of internal pressure, which is presumed to be a critical one for producing a wrinkle shape and rupture similar to the field NPS10 line pipe (Fig. 3).

The normal internal pressure ($p_i$) during main load test was chosen as either $0.30p_y$ or $0.15p_y$, where $p_y$ is the internal pressure required to yield the pipe material in the hoop or circumferential direction and for this pipe specimen, the value of $p_y$ was found to be 36.5 MPa (5294 psi). Specimens 1 and 2 were subjected to an internal pressure of $0.30p_y$ or 11.0 MPa (1600 psi), and Specimens 3 and 4 were subjected to an internal pressure of $0.15p_y$ or 5.5 MPa (800 psi), as shown in Table 1.

## 5 Test Results

**5.1 Load-Deformation Behavior.** The axial load-axial deformation behavior of all the four specimens is shown in Fig. 11. This figure shows that the axial load-axial deformation for all the four specimens were very similar. The normal internal pressure for specimens 1 and 2 was double of that for specimens 3 and 4. The maximum load capacity for specimens 3 and 4 were slightly higher than those obtained from specimens 1 and 2. However, the specimens 3 and 4 softened at a faster rate than the specimens 1

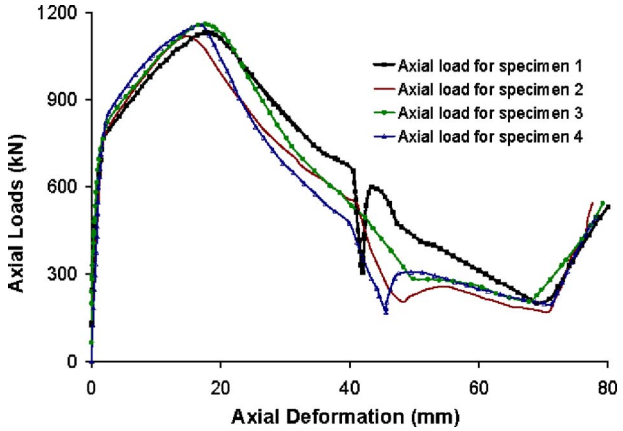


**Fig. 11 Axial load-axial deformation behavior of all specimens**

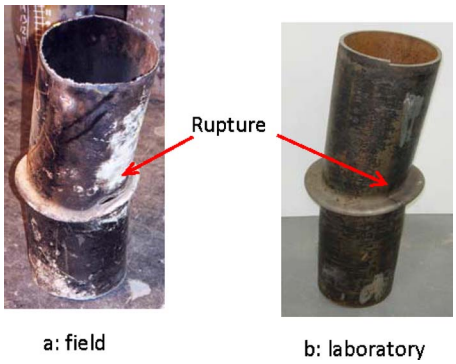


**Fig. 12 Comparison of field and lab specimens 2**

and 2 as the wrinkle formed and continued to grow, since the internal pressure for specimens 3 and 4 was relatively lower than for specimens 1 and 2.

Figures 7 and 8 show the load-deformation behaviors obtained from specimens 4 and 2, respectively. Specimen 4 was subjected to a lower internal pressures of $0.15p_y$, and specimen 2 was subjected to a relatively higher internal pressure, which was $0.30p_y$ (Table 1). In these figures, both the axial and lateral loads are shown to understand the interaction between these two loads. The first axial loading (load step 1) started at point A, and loading was continued in load control until the specimen yielded (point B). Then the axial loading was continued in the deformation control. The maximum axial load reached at point C, and axial deformation was continued until point D when the total axial deformation reached about 40 mm. The wrinkle initiated at point C, that is, at the maximum axial load. The wrinkle became visible by open eye soon after. The wrinkle continued to grow until point D when the axial deformation was discontinued.

In the next load step (load step 2), the lateral load was applied during path D-E-F followed by application of second axial deformation during the path E-F-G-H. The maximum lateral load reached at point E and as result, minimum axial load value reached at that point. Then the axial load value was increased gradually and as result, the lateral load value was reduced in path E-F even though no loading and unloading was done through the lateral loading jack. It is obvious that the wrinkle closed (surface of the pipe wall above the wrinkle came in contact with the surface of the pipe wall below the wrinkle) from inside of the pipe wall at point G. As a result, the axial load capacity began to increase as the axial deformation continued to increase monotonically (path G-H) during load step 3. The shape of the pipe wrinkle looked similar to the field pipe. The wrinkle shape of specimens 2 and 4 resembled best with that of field NPS10 line pipe, and the comparison between specimen 2 and the field pipe is shown in Fig. 12. At the end of load step 3, several small cracks appeared in all four specimens either at the top foot or at the crest of the wrinkle. The pipeline cleaning and inspection tool commonly known as "GeoPig," "Pig," or "SmartPig" is not able to pass this type of wrinkled pipeline segment, and thus, this type of wrinkle poses a threat to the normal pipeline operation. Therefore, the test specimen at this stage was considered to be failed, though no leak or rupture was observed at this stage. Then, the specimen was completely unloaded, and the water was drained out from the pipe specimen.

Next, the pressure test was conducted on each pipe specimen. The purpose was to study what might have happened in the field wrinkled NPS10 line pipe once the pipeline operation was being resumed after regular shutdown. The top end of the specimen was made free from all rotations and translations. The bottom end of the pipe specimen was restricted from vertical displacement only since the specimen was resting on the floor. The pipe specimen ruptured either at the top foot of the wrinkle or at the crest when the pressure was in the range of $0.14p_y$ and $0.17p_y$ (Table 1). Specimen 3 split into two pieces through the crest of the wrinkle (Fig. 13) when the pressure was only 6.1 MPa, which is equivalent to $0.17p_y$ (Table 1). An increase in pressure during the pressure test created tension in the pipe wall and as a result, the cracks which developed during the main load test opened up and thus, rupture occurred.

**5.2 Deformed Shape and Rupture.** The final deformed shapes of all the specimens before pressure tests are shown in Fig. 14. The specimens are arranged in their chronological order from left to right. The deformation shape of specimen 2 after the pressure test is compared with the field specimen in Fig. 12. As mentioned before, end rotations for specimen 1 could not be controlled in the desired manner and as a result, this specimen bent

**Fig. 13 Specimen 3 split into two pieces during the pressure test**


**Fig. 14 Shape of all specimens before the pressure tests**

much more than the other three specimens. Nevertheless, the shape of the wrinkle in this specimen was also similar to the field NPS10 line pipe (Fig. 14).

The test results shows that the levels of internal pressure ($0.15p_y$ and $0.30p_y$) chosen in this study did not influence the wrinkle shape and the location of rupture. The unloading of the internal pressure in load step 3 (during application of the second axial deformation), as was done for specimens 2 and 4, produced the wrinkle shape that is much closer to the field NPS10 line pipe and rupture occurred at the top foot of the wrinkle (Fig. 12). For the other two specimens (specimens 1 and 3), the internal pressure was not changed during load step 3 of the main load test and the rupture occurred at the crest of the wrinkle. In fact, specimen 3 separated into two pieces through the crest. Nevertheless, all the pipe specimens ruptured during pressure test when the pressure was in the range of $0.14–0.17p_y$ only and as a result, all the test specimens lost their structural integrity.

The test results show that the load histories that were applied to the laboratory test specimens are able to produce a wrinkle shape and rupture similar to that which occurred in the field NPS10 line pipe. Therefore, this study shows that the field wrinkled line pipe is vulnerable when it is subjected to a combined axial and lateral deformation history similar to those applied in the current study. It seems that the segment of the NPS10 field pipeline in the unstable slope might have developed a wrinkle due to soil movement in the direction of the longitudinal axis of the line pipe. Then, movement of the soil not aligned to the longitudinal axis of the line pipe created a lateral or oblique load in the wrinkle region. Finally, further axial load or deformation was applied on the wrinkled portion of the pipe in the direction of axis of the line pipe either during or before the shutdown took place, and this created a wrinkle shape that looks like a cowboy hat, as shown in Fig. 9(*c*). Then the pressure in the line pipe was reduced to zero as the pipeline operation was shut down for its maintenance. The field pipeline ruptured as soon as the internal pressure was being applied when it was being brought back to its normal operation.

**5.3 Strain History.** The primary objective of this study was to understand the probable load-deformation history similar to that which might have caused the wrinkle shape and rupture in the wrinkle of the NPS10 field line pipe. The other objective of this research was to understand the behavior of wrinkle growth and obtain the local strain history at the wrinkle location as the wrinkle grows to the limit. The "limit" in this context indicates a limit of the rupture failure or excessive cross sectional distortion that would threaten the integrity and operation of the energy pipelines. As mentioned before, electrical resistance strain gauges were installed in a staggered manner to capture the strain at every possible location of the wrinkle. Figure 15 shows the relative locations of various critical strain gauges relative to the crest and feet of the wrinkle. Strain gauges 14 and 20 were at the top and bottom feet of the wrinkle, whereas strain gauge 17 was at the crest of wrinkle. Strain gauge 11 was at about 30 mm away from the top foot of the wrinkle, and strain gauge 1 was far away (100 mm from the foot) from the wrinkle.

Figure 16 shows the strain plots obtained from the strain gauges at various critical locations of specimen 4. Similar strain behavior was observed from other specimens as well. The strain history differs from one location to another with respect to the crest or the foot of the wrinkle as the wrinkle grows and it can be seen in this figure. Since the foot of the wrinkle continues to be compressed as the specimens is loaded axially, the strain in that location continues to increase, and the maximum compressive strain was as high as 15% (Table 2 and Fig. 16). The strain at the crest of the wrinkle, however, continues to increase until the wrinkle initiates, that is, when the maximum load capacity is reached (point C in Figs. 7 and 8). The strain in this location begins to drop as the wrinkle continues to grow since the crest of the wrinkle goes to tension. The strain at locations either away (strain gauge 11) or far away (strain gauge 1) from the wrinkle zone becomes inactive since the strain does not increase any more once the wrinkle has initiated and plastic deformation localizes in the wrinkle only. Similar behavior was obtained from the other specimens as well. However, the maximum strain values differed slightly from one specimen to another (Table 2). The strain gauges were either removed before the application of the lateral load (load step 2) or did not function once the lateral load in load step 2 began. Therefore, the strain history shown in Fig. 16 is for load step 1 (first axial load) only.

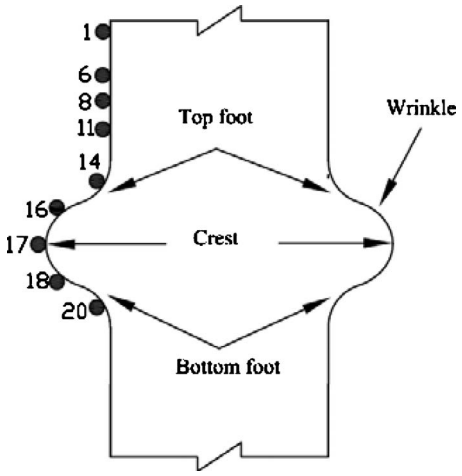


**Fig. 15 Relative locations of the strain gauges**

Figure 16 and Table 2 show that the local strain at the foot of the wrinkle can be very high and much higher than the strain limit values recommended by the current design standards [15–17], and the line pipe is very ductile since it does not rupture under monotonically increasing large axial deformation.

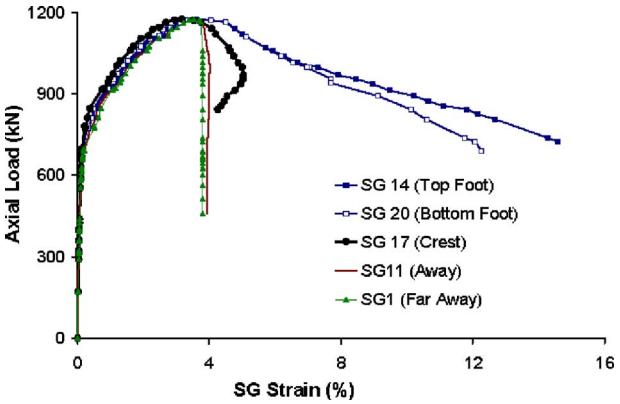


**Fig. 16 Axial load-strain behavior of specimen 4**

**Table 2 Test results**

| Specimen | Maximum strain (%) | | Maximum rotation (deg) | | Rupture at |
|---|---|---|---|---|---|
| | Foot | Crest | Top end | Bottom end | |
| 1 | 14.6 | 5.0 | 8.0 | 11 | Crest |
| 2 | 13.8 | 2.6 | 2.2 | 2.8 | Top foot |
| 3 | 15.2 | 4.5 | 3.8 | 2.1 | Crest |
| 4 | 15.0 | 6.1 | 2.3 | 3.3 | Top foot |

Note: Maximum strain value corresponds to the end of load step 1. Specimen 3 separated through the crest.

## 6 Conclusions

The following conclusions are made based on the experimental results obtained from this study. The conclusions made are specific to the pipe specimen and load history used in this study.

1. The line pipe used in this study is very ductile and does not rupture under application of large axisymmetric axial deformation.
2. The maximum local compressive strain values obtained after the end of load step 1 was 15%.
3. The combination of the axial and lateral loads applied to the wrinkled specimens is able to produce the wrinkle shape that looks similar to the one developed in the field NPS10 line pipe.
4. It seems that the levels of internal pressure ($0.15p_y$ and $0.30p_y$) chosen in this study did not influence the wrinkle shape and the location of the rupture much.
5. The unloading of internal pressure in load step 3, which is during application of the second axial deformation, however, produced the wrinkle shape and rupture, which correlate better with the field NPS10 line pipe.
6. All four specimens ruptured in the wrinkle region during the pressure test and when the internal pressure was only in the range of $0.14–0.17p_y$ and as a result, all the test specimens lost their structural integrity. In fact, specimen 3 split into two pieces through the crest. This study, therefore, states that the NPS10 field line pipe may have ruptured when the line pressure was being brought back to its normal level after its regular shutdown.

## Acknowledgment

The authors acknowledge the financial support received from the Natural Sciences and Engineering Research Council of Canada (NSERC).

## Nomenclature

$D$ = actual outside diameter of the pipe
$E$ = actual modulus of elasticity of the pipe steel
$P_a$ = axial load applied
$P_l$ = lateral load applied
$p_i$ = internal pressure applied by the fluid pump
$p_y$ = internal pressure that causes the yield stress of the pipe material
$t$ = actual thickness of the pipe wall
$\sigma_y$ = actual yield stress of the pipe material

## References

[1] Yukon Government, 2008. "Frequently Asked Questions: Oil and Gas Information," http://www.emr.gov.yk.ca/oilandgas/faq.html#pipe1
[2] Gresnigt, A. M., 1986, "Plastic Design of Buried Steel Pipelines in Settlement Areas," Heron, **31**(4), pp. 40–51.
[3] Yoosef-Ghodsi, N., Kulak, G. L., and Murray, D. W., 1995. "Some Test Results for Wrinkling of Girth-Welded Linepipe," Proceedings of the 14th ASME International Conference on Offshore Mechanics and Arctic Engineering, Copenhagen, Denmark, pp. 379–388.
[4] Dorey, A. B., Murray, D. W., Cheng, J. J. R., Grondin, G. Y., and Zhou, Z. J., 1999, "Testing and Experimental Results for NPS30 Pipe under Combined Loads," ASME Paper No. OMAE99/PIPE-5022.
[5] Das, S., Cheng, J. J. R., Murray, D. W., Wilkie, S. A., and Zhou, Z. J., 2000, "Laboratory Study of Wrinkle Development and Strains for NPS12 Line Pipe," Proceedings of the Third International Pipeline Conference, Calgary, Canada, pp. 909–915.
[6] Jayadevan, K. R., Ostby, E., and Thaulow, C., 2004, "Strain Based Fracture Mechanics Analysis of Pipelines," Proceedings of the International Conference on Advances in Structural Integrity, Bangalore, India, Paper No. ICAS/04-0198.
[7] Vitali, L., Bartolini, L., Askheim, D., Reek, R., and Levold, E., 2005, "Hotpipe Jl Project Experimental Test and FE Analyses," Proceedings of the 24th ASME International Conference on Offshore Mechanics and Arctic Engineering, Halkidiki, Greece, pp. 715–729.
[8] Dorey, A. B., Murray, D. W., and Cheng, J. J. R., 2006, "Critical Buckling Strain Equations for Energy Pipelines—A Parametric Study," ASME J. Offshore Mech. Arct. Eng., **128**(3), pp. 248–255.
[9] Zhang, Y., and Das, S., 2008, "Failure of X52 Wrinkled Pipelines Subjected to Monotonic Axial Deformation," ASME J. Pressure Vessel Technol., **130**(2), pp. 1–7.
[10] Mohareb, M., Alexander, S. D. B., Kulak, G. L., and Murray, D. W., 1993, "Laboratory Testing of Line Pipe to Determine Deformation Behavior," *Proceedings of the 12th International Conference on Offshore Mechanics and Arctic Engineering: Pipeline Technology*, ASME, New York, Vol. V, pp. 109–114.
[11] Das, S., Cheng, J. J. R., Murray, D. W., Wilkie, S. A., and Zhou, Z. J., 2001, "Wrinkle Behavior Under Cyclic Strain Reversals in NPS12 Pipe," Proceedings of the 20th ASME International Conference on Offshore Mechanics and Arctic Engineering, Rio de Janeiro, Brazil, pp. 129–138.
[12] Das, S., Cheng, J. J. R., and Murray, D. W., 2007, "Prediction of Fracture Life of Wrinkled Steel Pipe Subject to Low Cycle Fatigue Load," Can. J. Civ. Eng., **34**, pp. 1131–1139.
[13] Das, S., Cheng, J. J. R., and Murray, D. W., 2002, "Fracture in Wrinkled Linepipe Under Monotonic Loading," Proceedings of the Fourth International Pipeline Conference, Calgary, Canada, Paper No. IP C2002-C27097.
[14] 2008, *Specifications for Line Pipe: API 5L*, American Petroleum Institute, Washington, DC.
[15] 2007, *Oil and Gas Pipeline Systems: Z662*, Canadian Standard Association, Etobicoke, Canada.
[16] 2004, *Code of Practice for Pipelines, Part 1: Steel Pipelines on Land*, British Standard Institution, London, UK.
[17] 2007, *Offshore Standard OS-F101: Submarine Pipeline Systems*, Det Norske Veritas, Veritasveien, Hovik, Norway.